Materials and Design 32 (2011) 4088–4093

Contents lists available at ScienceDirect

Materials and Design

journal homepage: www.elsevier.com/locate/matdes

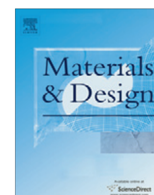

Technical Report

Investigated optical and elastic properties of Porous silicon: Theoretical study

Y. Al-Douri [a,*], N.M. Ahmed [b], N. Bouarissa [c], A. Bouhemadou [d,e]

[a] Institute of Nano Electronic Engineering, University Malaysia Perlis, 01000 Seriab Kanagar, Perlis, Malaysia
[b] School of Physics, Universiti Sains Malaysia, 11800 Penang, Malaysia
[c] Department of Physics, Faculty of Science, King Khalid University, Abha, P.O. Box 9004, Saudi Arabia
[d] Laboratory for Developing New Materials and Their Characterization, Department of Physics, Faculty of Science, University of Setif, 19000 Setif, Algeria
[e] Department of Physics, Faculty of Science, King Saud University, P.O. Box 2455, Riyadh 11451, Saudi Arabia

ARTICLE INFO

Article history:
Received 8 November 2010
Accepted 5 March 2011
Available online 12 March 2011

ABSTRACT

Compatibility between experimental and theoretical works is achieved. Empirical Pseudopotential Method (EPM) is used to calculate the energy gap of Si which is found to be indirect. Features such as refractive index, optical dielectric constant, bulk modulus, elastic constants and short-range force constants have been investigated. In addition to the shear modulus, Young's modulus, Poisson's ratio and Lame's constants for both bulk Si ($p = 0\%$) and Porous silicon (PS) are derived. The calculated results are found to be in good agreement with other experimental and theoretical ones. Also, the Debye temperature of PS is estimated from the average sound velocity. To our knowledge, the optical properties using specific models and elasticity of PS are reported for the first time.

© 2011 Elsevier Ltd. All rights reserved.

1. Introduction

Porous silicon (PS) is a special composite material consisting of pores and silicon backbone networks. It has a broad range of applications due to its high ratio of surface atoms that determine the high tunability of the PS in many properties such as dielectric constant [1,2], band gap [3] and chemical reactivity [4,5].

The efficient luminescence at room temperature in PS reported by Canham [6] has provoked great interest due to its potential for optoelectronic applications. Progress in PS optoelectronics depends on the understanding of the operating principles of PS device structures.

According to the model proposed by Canham [6,7], the recombination of electron–hole pairs occurs within nanometer silicon wires and their energy gaps become larger than that of bulk Si (quantum confinement effect). This model, modified by Koch et al. [8], suggests that electron–hole pairs are photo-excided in nanometer silicon particles and recombined via Si intrinsic surface states.

Several models have been proposed for studying the transport of carriers in PS based metal/PS/c-Si device structures [9–13]. To explain the experimental results, these models assume either that the reverse current is determined by the surface transport mechanism of hopping [11], or with carrier generation in surface states at the boundary between Porous silicon and c-Si substrate [10]. It was found that the forward current–voltage (I–V) dependence exhibits a relatively short exponential region with a quality factor of 4 or higher [10–13]. Pan et al. [14] have developed a method to characterize the dielectric properties of PS as a function of its porosity and the surface oxidation that are adjustable to experiment.

Besides, Milani et al. [15] have surveyed optoelectronic effects in PS using experimental measurements of photoluminescence (PL), current–voltage, surface resistance and specular reflectance of PS samples prepared with increasing etching time. These measurements have clarified the relationship between the observed behavior and porosity, and showed an increase of the band gap from 1.83 to 2 eV.

Porous materials are used in many areas of applied science and engineering and have taxonomies based on different criteria such as pore size, pore shape, materials and production types. Cicek and Celik [16] have proposed a decision aid mechanism based on fuzzy axiomatic design (FAD) to select adequate form of porous materials in marine systems design, and they addressed use of porous materials in plate type heat exchanger design to demonstrate the proposed model. Edwards [17] had chosen the optimal material and manufacturing process combination that regards a novel idea. Besides the feasible applications of this approach in engineering component design, the increasing complexity of technical system (i.e. energy plant, offshore, etc.) requires great potential, and the material selection of components is one of the most challenging issues in the design and development of technical systems. Furthermore, various studies have been performed to help address the issue of material selection. There are few methodological approaches towards solution of the problem as fuzzy knowledge based decision support system [18].

Although there were reviews which have been published throughout the past years, there exists no detailed study

* Corresponding author. Tel: +60 4 9775021; fax: +60 4 9798578.
E-mail address: yarub@unimap.edu.my (Y. Al-Douri).

0261-3069/$ - see front matter © 2011 Elsevier Ltd. All rights reserved.
doi:10.1016/j.matdes.2011.03.010

adequately documenting the optical properties using specific models, the structural properties, elastic properties and Debye temperature parameters as a function of porosity. This is due to the large number of the independent parameters (energy gap, bulk modulus, elastic constants and shear modulus), the chemistry and pore formation mechanisms that remain largely unknown. Refractive index, optical dielectric constant, bulk modulus, elastic constants and short-range force constants are investigated. Also, shear modulus, Young's modulus, Poisson's ratio and Lame's constants for both bulk Si and PS are derived. The Debye temperature of PS is estimated from the average sound velocity. Additionally, the optical properties and elasticity of PS are reported for the first time using the Empirical Pseudopotential Method (EPM).

The paper is organized as follows. In the following section the computational method is used in the present work. Section 3 is devoted to the presentation of our results comparing with previous calculations and experimental studies. A conclusion of the present work is given in Section 4.

2. Computational method

Using the Empirical Pseudopotential Method (EPM), the symmetric and antisymmetric pseudopotential form factors have been adjusted in order to fit the experimental energy band gaps of bulk and PS which are given in Table 1. Adjustments to the specific pseudopotential form factors are made using a nonlinear least-squares [21] fitting procedure. The lattice constant used for the bulk Si is 5.431 Å. The final adjusted symmetric and antisymmetric pseudopotential form factors of bulk Si and PS are listed in Table 1. Using the symmetric and antisymmetric pseudopotential form factors at $G(1\,1\,1)$, we have calculated the polarity α_p according to the Vogl [22] definition,

$$\alpha_P = -V_A(3)/V_S(3) \tag{1}$$

where $V_S(3)$ and $V_A(3)$ in Eq. (1) are the symmetric and antisymmetric pseudopotential form factors at $G(1\,1\,1)$, respectively. The pseudopotential Hamiltonian used for our calculation is given by

Table 1
Energy gap and adjusted pseudopotential form factors for bulk Si and PS.

Porous silicon (%)	Energy gap E_g (eV)	
	Cal.	Others
0	1.11	1.11[a,b]
27	1.40	–
33	1.45	–
43	1.56	–
58	1.59	–
65	1.78	–
73	1.80	–
75	1.85	–
88	1.88	–

	Form factors (Ry)					
	$V_s(3)$	$V_s(8)$	$V_s(11)$	$V_a(3)$	$V_a(4)$	$V_a(11)$
0	−0.21	0.04	0.08	0.0	0.0	0.0
27	−0.223679	0.046944	0.073340	0.0	0.0	0.0
33	−0.223678	0.046944	0.073340	0.0	0.0	0.0
43	−0.223677	0.046944	0.073340	0.0	0.0	0.0
58	−0.223676	0.046944	0.073341	0.0	0.0	0.0
65	−0.223675	0.046943	0.073341	0.0	0.0	0.0
73	−0.223672	0.046942	0.073342	0.0	0.0	0.0
75	−0.223668	0.046941	0.073343	0.0	0.0	0.0
88	−0.223661	0.046938	0.073345	0.0	0.0	0.0

[a] Ref. [19] exp.
[b] Ref. [20].

$$H = -\left(\frac{\hbar}{2m}^{2}\right)\nabla^2 + V(r), \tag{2}$$

where $V(r)$ is the pseudopotential that can be expanded in reciprocal lattice vectors G. For the zinc-blende structure, this yields [23]

$$V(r) = \sum_G (V_G^S \cos G.\tau + iV_G^A \sin G\cdot\tau)e^{-iG\cdot\tau}, \tag{3}$$

where $\tau = \tau_1 = -\tau_2 = \frac{1}{2}a(1\,1\,1)$ and a is the lattice constant. V_G^S and V_G^A are symmetric and antisymmetric pseudopotential form factors of an end-point binary compound and can be written in terms of the atomic potentials as

$$V_G^S = \frac{1}{2}[V_1(G) + V_2(G)],$$
$$V_G^A = \frac{1}{2}[V_1(G) - V_2(G)]. \tag{4}$$

The form factors in Eq. (4) are adjusted empirically by fitting the calculated band structure to the experimental data. They depend on the magnitudes of G. As in most of the EPM calculations, cutoff value of

$$|G|^2 = 11(2\pi/a)^2$$

is used. The contribution to the summation in Eq. (3) from terms beyond this cutoff $|G|^2$ is small and can be neglected.

Using the calculated polarities, the transverse effective charge e_T^* has been estimated from the relation [20]

$$e_T^* = -\Delta z + \frac{8\alpha_P}{1+\alpha_P^2} \tag{5}$$

where Δz is the differences of the atomic number.

3. Results and discussion

The increasing of the band gap from 1.4 to 1.88 eV with increasing the porosity in the range of 27–88% is observed. Fig. 1 shows the variation of the energy gap with the porosity percentage. A linear increase of band gap from 1.4 to 1.88 eV with rising of porosity of PS films in the range of 27–88% is noticed. This is due to atomic arrangement, mechanical behavior and quantum confinement of carriers in the PS microcrystallites, causing the widening of the Si band gap.

The refractive index n is a very important physical parameter that is related to the microscopic atomic interactions. It represents a fundamental physical aspect that characterizes their optical and

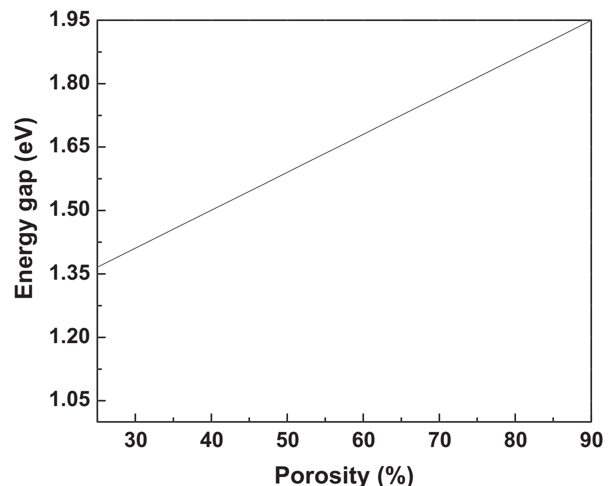

Fig. 1. Variation of energy gap versus porosity percentage for Porous silicon (PS).

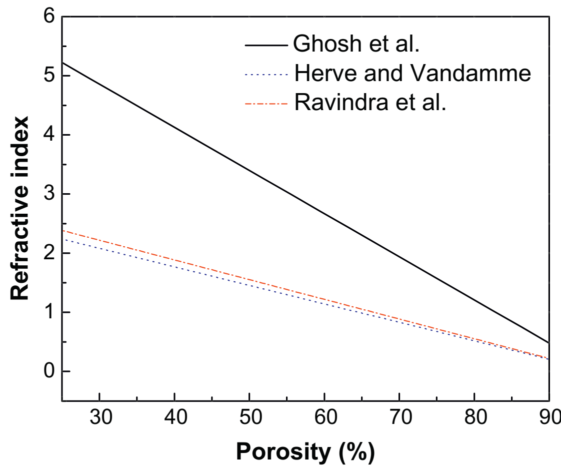

Fig. 2. Variation of refractive index versus porosity percentage for Porous silicon (PS), using different models.

electronic properties. Knowledge of the n is essential for devices such as photonic crystals, wave guides, solar cells and detectors [24]. On the other hand, n is closely related to the energy band structure of the material. Consequently, many attempts have been made in order to relate the refractive index and the energy gap E_g through simple relationships [25–30]. However, these relations of n are independent of temperature and incident photon energy. Ravindra et al. [30] have suggested a linear form of n as a function of E_g:

$$n = \alpha + \beta E_g \tag{6}$$

where $\alpha = 4.048$ and $\beta = -0.62\ \text{eV}^{-1}$.

To be inspired by a simple physics of light refraction and dispersion, Herve and Vandamme [31] proposed an empirical relation as follows:

$$n = \sqrt{1 + \left(\frac{A}{E_g + B}\right)^2} \tag{7}$$

where $A = 13.6$ eV and $B = 3.4$ eV. On the other hand, Ghosh et al. [32] have took a different approach to the problem by considering the band structural and quantum-dielectric formulations of Penn [33] and Van Vechten [34], respectively. Introducing A as the contribution from the valence electrons and B as a constant additive to the lowest band gap E_g, the expression for the high-frequency refractive index is written as:

$$n^2 - 1 = \frac{A}{(E_g + B)^2} \tag{8}$$

where $A = 8.2E_g + 134$, $B = 0.225E_g + 2.25$ and $(E_g + B)$ refers to an appropriate average energy gap of the material. Using the three models mentioned above, the n has been calculated as a function of the percentage porosity. Thus, these three models of variation of n with energy gap have been calculated. Our results for PS are displayed in Fig. 2. The calculated refractive indices of the end-point compounds are listed in Table 2, and showed good accordance with experimental result. Also, the calculated values of the high-frequency dielectric constant (ε_∞) that were obtained using the relation $\varepsilon_\infty = n^2$ [38] are given in Table 2 and showed good agreement with experimental value. From Fig. 2 one can see that n decreases almost linearly with the percentage porosity for the three models and that the refractive index for higher E_g tends to shift towards the blue green[1].

[1] For interpretation of color in Fig. 2, the reader is referred to the web version of this article.

Table 2
Calculated refractive indices (n) and high-frequency optical dielectric constant (ε_∞) for bulk Si and PS using: Ravindra et al. [30], Hervé and Vandamme [31] and Ghosh et al. [32] models.

Porous silicon (%)	n	ε_∞
0	3.395[a], 3.177[b], 3.432[c], 3.882[d]	11.526[a], 10.093[b], 11.778[c], 11.68[e]
27	3.216[a], 3.004[b], 3.202[c]	10.342[a], 9.024[b], 10.252[c]
33	3.185[a], 2.977[b], 3.162[c]	10.144[a], 8.862[b], 9.998[c]
43	3.116[a], 2.918[b], 3.078[c]	9.709[a], 8.514[b], 9.474[c]
58	3.098[a], 2.903[b], 3.056[c]	9.597[a], 8.427[b], 9.339[c]
65	2.98[a], 2.809[b], 2.927[c]	8.880[a], 7.890[b], 8.567[c]
73	2.968[a], 2.8[b], 2.914[c]	8.809[a], 7.84[b], 8.491[c]
75	2.937[a], 2.776[b], 2.883[c]	8.625[a], 7.706[b], 8.311[c]
88	2.918[a], 2.763[b], 2.864[c]	8.514[a], 7.634[b], 8.202[c]

[a] Ref. [30].
[b] Ref. [31].
[c] Ref. [32].
[d] Ref. [35,36] exp.
[e] Ref. [37] exp.

The bulk modulus (B_0) for both bulk Si and PS is also calculated using the Al-Douri et al. [39] relation:

$$B_0 = (30 + 10\lambda)(P_t^{1/2}/E_{g\Gamma-X})/3 \tag{9}$$

where P_t is the transition pressure, $E_{g\Gamma-X}$ is the energy gap along $\Gamma - X$ and λ is a parameter appropriate for the group-IV = 0, III–V = 1 and II–VI = 5 semiconductors. Our results of B_0 are listed in Table 3 along with the experimental and theoretical data in the literature. Our result concerning B_0 for bulk Si is in good agreement with the experimental one reported in Ref. [40]. Moreover, it agrees very well with the theoretical calculations [41,42]. The variation of B_0 as a function of percentage porosity is plotted in Fig. 3. Note that as the percentage porosity increases, B_0 decreases gradually. The

Table 3
Bulk modulus, elastic constants, bond-stretching force constant and bond-bending force constant for bulk Si and PS.

Porous silicon (%)	Bulk modulus B_0 (GPa) Cal.	Others
0	100.7	98[a], 100[b], 92[c]
27	97.85	–
33	77.10	–
43	71.66	–
58	70.31	–
65	62.81	–
73	62.11	–
75	60.43	–
88	59.46	–

Porous silicon (%)	C_{11} (10^{11} dyn/cm^2) Cal.	C_{11} Exp.[d]	C_{12} (10^{11} dyn/cm^2) Cal.	C_{12} Exp.[d]	C_{44} (10^{11} dyn/cm^2) Cal.	C_{44} Exp.[d]	α (N/M) Cal.	α Exp.[d]	β (N/m) Cal.	β Exp.[d]
0	17.9	16.57	7.71	6.39	8.16	7.96	55.71	48.50	13.84	13.81
27	5.65	–	2.42	–	2.58	–	22.10	–	5.53	–
33	4.74	–	2.03	–	2.17	–	19.20	–	4.80	–
43	3.29	–	1.41	–	1.50	–	14.34	–	3.59	–
58	2.99	–	1.28	–	1.37	–	13.28	–	3.32	–
65	1.70	–	0.73	–	0.78	–	8.47	–	2.11	–
73	1.61	–	0.69	–	0.74	–	8.10	–	2.02	–
75	1.40	–	0.60	–	0.64	–	7.24	–	1.81	–
88	1.29	–	0.55	–	0.59	–	6.76	–	1.70	–

[a] Ref. [40] exp.
[b] Ref. [41].
[c] Ref. [42].
[d] Ref. [43].

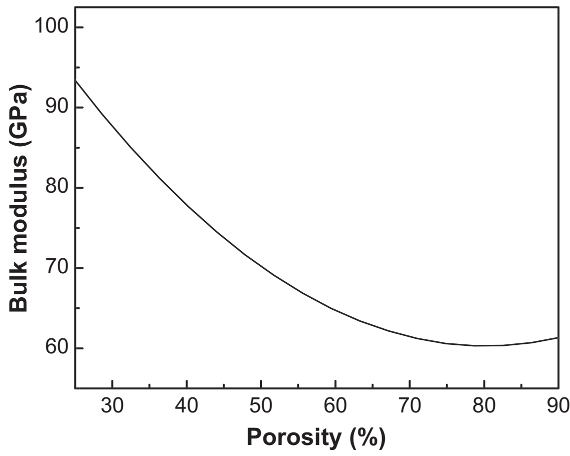

Fig. 3. Variation of bulk modulus versus porosity percentage for Porous silicon (PS).

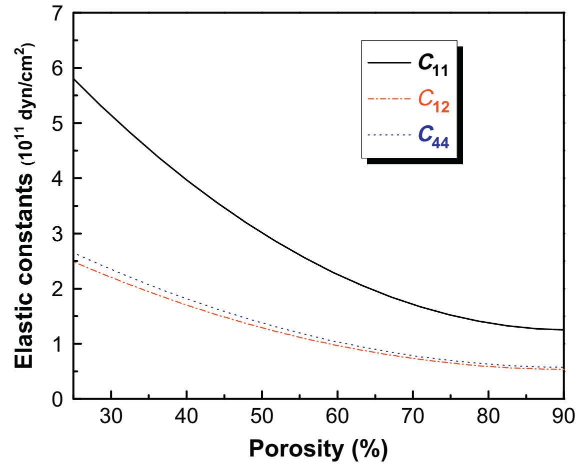

Fig. 4. Variation of elastic constants versus porosity percentage for Porous silicon (PS).

decrease of B_0 with increasing porosity suggests that PS becomes more compressible with increasing percentage porosity.

We now turn our attention to the elastic properties. In this respect, the elastic constants namely C_{11}, C_{12} and C_{44} have been calculated following the same procedure used by Bouarissa [44] that was based essentially on the work of Baranowski [45], where C_{11}, C_{12} and C_{44} are expressed as,

$$C_{11} = \frac{\sqrt{3}\hbar^2}{4d^5m}\left(1-\alpha_p^2\right)^{\frac{1}{2}}[4.37(5+\lambda)(1-\alpha_p^2) - 0.6075] \quad (10)$$

$$C_{12} = \frac{\sqrt{3}\hbar^2}{4d^5m}\left(1-\alpha_p^2\right)^{\frac{1}{2}}[4.37(3-\lambda)(1-\alpha_p^2) + 0.6075] \quad (11)$$

$$C_{44} = \frac{\sqrt{3}}{4d}(\alpha+\beta) - 0.136SC_0 - C\xi^2 \quad (12)$$

In Eqs. (10)–(12), d is the nearest neighbor distance, λ is a dimensionless parameter which has a constant value of 0.738 [45] and l is the electron mass. The quantities α and β in Eq. (12) are the short-range force constants. They represent the bond-stretching and bond-bending force constants, respectively and are expressed as [46],

$$\alpha = \frac{d}{\sqrt{3}}(C_{11}+3C_{12}) + \frac{d}{3\sqrt{3}}(1.473SC_0) \quad (13)$$

$$\beta = \frac{d}{\sqrt{3}}[(C_{11}-C_{12}) - 0.053SC_0] \quad (14)$$

The parameter ξ is the internal-strain parameter. The quantities S and C_0 are obtained using the following expressions,

$$S = \frac{Z^{*2}}{\varepsilon(0)} \quad (15)$$

$$C_0 = \frac{e^2}{d^4} \quad (16)$$

S is an effective charge parameter, C_0 has the dimensions of an elastic constant and z^* is the effective charge. More details about the determination of the quantities C, ξ and $z^*$are given in Ref. [46]. $\varepsilon(0)$ is the static dielectric constant.

Our results concerning C_{11}, C_{12} and C_{44} for bulk Si and PS are given in Table 3 including the experimental and theoretical data for comparison. Generally, our results agree reasonably well with those reported in the literature.

The variation of the elastic constants C_{11}, C_{12} and C_{44} as a function of the porosity is displayed in Fig. 4. One can observe that all the studied elastic constants decrease non-linearly with increasing the porosity. However, it should be noted that the following behavior is seen. Qualitatively, the trends of elastic constants of PS are similar. From the quantitative point of view, the elastic constants show considerable differences according to the porosity changes, where they have larger values when Si has low porosity and smaller values when Si has high porosity on the entire range of porosity.

The calculated bond-stretching and bond-bending force constants as well as the internal-strain parameter for the bulk Si and PS with available data in the literature are shown in Table 3. From Table 3, one can see that our results agree well with those obtained experimentally [40,43]. For PS, the quantities α and β are seen to have larger values when PS has low porosity and smaller values when PS has high porosity.

The variation of the bond-stretching and bond-bending force constants as a function of the porosity are plotted in Fig. 5. According to this figure, one can see that increasing the porosity leads to a decrease of both force constants. This trend is almost similar to those shown by the elastic constants that imply the PS could provide more opportunities to obtain desired elastic and short-range force constants with changing the porosity percentage.

Having calculated the Young's modulus E, bulk modulus B_0 and shear modulus G, one can calculate the Debye temperature, which is an important fundamental parameter closely related to many physical properties such as elastic constants, specific heat and

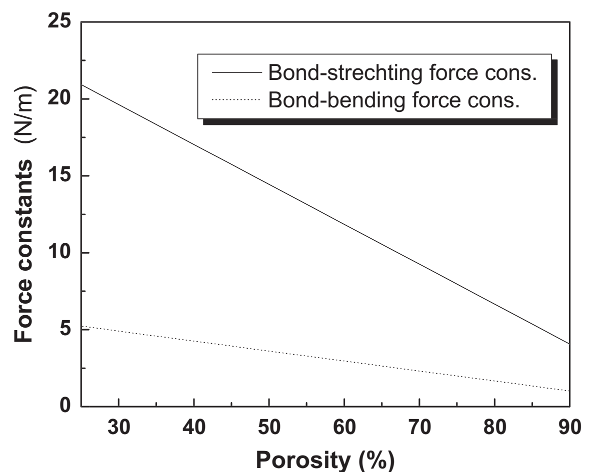

Fig. 5. Variation of force constants versus porosity percentage for Porous silicon (PS).

Table 4
Calculated shear modulus (G), Young's modulus (E), Poisson's ratio (υ), Lame's constants (λ and μ), density (ρ), longitudinal (v_l), transverse (v_t), average sound velocity (v_m) and Debye temperature (θ_D) for bulk Si and PS.

Porous silicon (%)	G (GPa)	E (GPa)	υ	λ (GPa)	μ (GPa)
0	67.55657	168.50515	0.24714	66.02895	67.55657
	52[a]	185[a]	0.28[a]	64[b]	79.6[b]
27	21.38154	53.28389	0.24603	20.7123	21.38154
33	17.96584	44.75953	0.24568	17.35611	17.96584
43	12.4367	31.00013	0.24632	12.07553	12.4367
58	11.34003	28.24826	0.24551	10.93998	11.34003
65	6.44682	16.06332	0.24583	6.23546	6.44682
73	6.11552	15.23128	0.2453	5.88965	6.11552
75	5.30065	13.209	0.24598	5.1329	5.30065
88	4.89319	12.18488	0.24509	4.70454	4.89319
	ρ (g/cm^3)	v_l (m/s)	v_t (m/s)	v_m (m/s)	θ_D (K)
0	2.32907	9293.0995	5385.7092	6961.2197	763.243423
	2.3290[c]	8790[d]	5410[d]	6573.3[e]	645[f]
27	1.16231	7389.9686	4289.0334	5541.4547	481.926708
33	1.0464	7136.1579	4143.5668	5352.8418	449.50493
43	0.84027	6631.1948	3847.1881	4971.1194	388.011073
58	0.79351	6509.129	3780.3399	4883.299	373.950912
65	0.56561	5815.5353	3376.0992	4361.6319	298.358054
73	0.54693	5756.0285	3343.8925	4319.1729	292.164484
75	0.50369	5589.0827	3244.0135	4191.2147	275.832129
88	0.47992	5494.9651	3193.1031	4124.0868	267.075223

[a] Ref. [48] exp.
[b] Ref. [49] exp.
[c] Ref. [50,51] exp,
[d] Ref. [52] exp.
[e] Ref. [53] exp.
[f] Ref. [54] exp.

melting temperature. We have estimated the Debye temperature θ_D of bulk Si and PS from the average sound velocity, v_m, by the following equation [47]:

$$\theta_D = \frac{h}{k_B}\left[\frac{3}{4\pi V_a}\right]^{1/3} v_m \quad (17)$$

where h is the Plank's constant, k_B, the Boltzman's constant and V_a is the atomic volume. The average sound velocity in the polycrystalline material is given by:

$$v_m = \left[\frac{1}{3}\left(\frac{2}{v_t^3}+\frac{1}{v_l^3}\right)\right]^{\frac{1}{3}} \quad (18)$$

where v_l and v_t are the longitudinal and transverse sound velocity obtained using the shear modulus G and the bulk modulus B_0 from Navier's equation [47]:

$$v_l = \left(\frac{3B+4G}{3\rho}\right)^{1/2} \quad \text{and} \quad v_t = \left(\frac{G}{\rho}\right)^{\frac{1}{2}} \quad (19)$$

The calculated sound velocity and Debye temperature as well as the density for PS are given in Table 4. It is shown that our calculated results of 0% PS are in good accordance with experimental values [48–54]. For PS, the correlation of the calculated values with porosity is proportional inversely. Future works will test our calculated results. The present results stand, therefore, as reliable predictions for these parameters.

4. Conclusions

Increasing the band gap of Porous silicon (PS) with porosity is reported in this work and can be supported by quantum confinement based model of luminescence in PS. Based on Empirical Pseudopotential Method (EPM); it is shown that Si is an indirect band gap. The results of the optical and elastic properties for PS are investigated. A good agreement with experimental and theoretical data for energetic transitions and elastic properties are obtained. The sound velocity and Debye temperature are estimated and showed a good accordance with experimental results.

Acknowledgment

This work has been achieved using FRGS grant numbered: 9003-00249. One of us (Y.A.) would like to acknowledge TWAS-Italy, to support his visit to JUST-Jordan under TWAS-UNESCO Associateship.

References

[1] Sun CQ, Sun XW, Tay BK, Lau SP, Huang H, Li S. Dielectric suppression and its effect on photoabsorption of nanometric semiconductors. J Phys D 2001;34:2359–62.
[2] Pan LK, Huang HT, Sun CQ. Dielectric relaxation and transition of porous silicon. J Appl Phys 2003;94:2695–700.
[3] Pan LK, Sun CQ. Coordination imperfection enhanced electron–phonon interaction. J Appl Phys 2004;95:3819–21.
[4] Pan LK, Ee YK, Sun CQ, Yu GQ, Zhang QY, Tay BK. Band-gap expansion, core-level shift, and dielectric suppression of porous silicon passivated by plasma fluorination. J Vac Sci Technol B 2004;22:583–7.
[5] Li YY, Cunin F, Link JR, Gao T, Betts RE, Reiver SH, et al. Polymer replicas of photonic porous silicon for sensing and drug delivery applications. Science 2003;299:2045–7.
[6] Canham LT. Silicon quantum wire array fabrication by electrochemical and chemical dissolution of wafers. Appl Phys Lett 1990;57:1046–8.
[7] Hybersen MS. Absorption and emission of light in nanoscale silicon structures. Phys Rev Lett 1994;72:1514–7.
[8] Koch F, Petrova V, Muschik T, Nikolov A, Gavrilenko V. Sensitivity of porous silicon photoluminescence to low concentrations of CH_4 and CO. Mater Res Soc Symp Proc 1993;283:197.
[9] Balagurov LA, Yarkin DG, Petrova EA, Orlov AF, Andrushin Ya S. Highly sensitive porous silicon based photodiode structures. J Appl Phys 1997;82:4647–50.
[10] Dimitrov DB. Current–voltage characteristics of porous-silicon layers. Phys Rev B 1995;51:1562–6.
[11] Deresmes D, Marisael V, Stievenard D, Ortega C. Electrical behavior of aluminium-porous silicon junctions. Thin Solid Films 1995;255:258–61.
[12] Chen Z, Lee TY, Bosman G. Electrical characterization and modeling of wide band gap porous silicon p–n diodes. J Appl Phys 1994;76:2499–504.
[13] Timoshenko VY, Kashkarov PK, Matveeva AB, Konstantinova EA, Flietner H, Dittrich Th. Influence of photoluminescence and trapping on the photovoltage at the por-Si/p-Si structure. Thin Solid Films 1996;276:216–8.

[14] Pan LK, Sun CQ, Li CM. Estimating the extent of surface oxidation by measuring the porosity dependent dielectrics of oxygenated porous silicon. Appl Surf Sci 2005;240:19–23.
[15] Milani ShD, Dariani RS, Mortezaali A, Daadmehr V, Robbie K. The correlation of morphology and surface resistance in porous silicon. J Optoelectron Adv Mater 2006;8:1216–20.
[16] Cicek K, Celik M. Selection of porous materials in marine system design: the case of heat exchanger aboard ships. Mater Des 2009;30:4260–6.
[17] Edwards KL. Designing of engineering components for optimal materials and manufacturing process utilisation. Mater Des 2003;24:355–66.
[18] Amen R, Vomacka P. Case-based reasoning as a tool for materials selection. Mater Des 2001;22:353–8.
[19] Tsidilkovski IM. Band structure of semiconductors. Oxford: Pergamon Press; 1982.
[20] Humphreys RG, Rossler V, Cardona M. Indirect exciton fine structure in GaP and the effect of uniaxial stress. Phys Rev B 1978;18:5590–605.
[21] Kobayasi T, Nara H. Properties of nonlocal pseudopotential of Si and Ge optimized under full interdependence among potential parameters. Bull Coll Med Sci, Tohoku Univ 1993;2:7–16.
[22] Vogl P. Dynamical effective charges in semiconductors: a pseudopotential approach. J Phys C 1978;11:251.
[23] Cohen ML, Bergstresser TK. Band structures and pseudopotential form factors for fourteen semiconductors of the diamond and zinc-blende structures. Phys Rev 1966;141:789–96.
[24] Ravindra NM, Ganapathy P, Choi J. Energy gap–refractive index relations in semiconductors – an overview. Infrared Phys Technol 2007;50:21–9.
[25] Moss TS. A relationship between the refractive index and the infra-red threshold of sensitivity for photoconductors. Proc Phys Soc B 1950;63:167.
[26] Gupta VP, Ravindra NM. Comments on the moss formula. Phys Status Solidi B 1980;100:715–9.
[27] Ruoff AL. Pressure dependence of the refractive index of diamond, cubic silicon carbide and cubic boron nitride. Mater Res Soc Symp Proc 1984;22: 287.
[28] Reddy RR, Anjaneyulu S, Samara CLN. Relationship between energy gap, refractive index, bond energy and the szigeti charge in polyatomic binary compounds and semiconductors. J Phys Chem Solid 1993;54:635–7.
[29] Herve P, Vandamme LKJ. General relation between refractive index and energy gap in semiconductors. Infrared Phys Technol 1993;35:609–15.
[30] Ravindra NM, Auluck S, Srivastava VK. On the penn gap in semiconductors. Phys Status Solidi B 1979;93:K155–60.
[31] Herve PJL, Vandamme LKJ. Empirical temperature dependence of the refractive index of semiconductors. J Appl Phys 1995;77:5476–7.
[32] Ghosh DK, Samanta LK, Bhar GC. A simple model for evaluation of refractive indices of some binary and ternary mixed crystals. Infrared Phys 1984;24: 43–7.
[33] Penn DR. Wave-number-dependent dielectric functions of semiconductors. Phys Rev 1962;128:2093–7.
[34] Van Vechten JA. Quantum dielectric theory of electronegativity in covalent systems. I. Electronic dielectric constant. Phys Rev 1969;182:891–905.
[35] Aspnes DE, Theeten JB. Spectroscopic analysis of the interface between Si and its thermally grown oxide. J Electrochem Soc 1980;127:1359–65.
[36] Palik ED. Handbook of optical constants of solids. Boston: Academic Press; 1985.
[37] Gray PR, Hurst PJ, Lewis SH, Meyer RG. Analysis and design of analog integrated circuits. New York: Wiley; 2009.
[38] Samara GA. Temperature and pressure dependences of the dielectric constants of semiconductors. Phys Rev B 1983;27:3494–505.
[39] Al-Douri Y, Abid H, Aourag H. Calculation of bulk moduli of semiconductor compounds. Physica B 2002;322:179–82.
[40] Cohen ML. Calculation of bulk moduli of diamond and zinc-blende solids. Phys Rev B 1985;32:7988–91.
[41] Lam PK, Cohen ML, Martinez G. Analytic relation between bulk moduli and lattice constants. Phys Rev B 1987;35:9190–4.
[42] Al-Douri Y, Abid H, Aourag H. Correlation between the bulk modulus and the charge density in semiconductors. Physica B 2001;305:186–90.
[43] Martin RM. Elastic properties of ZnS structure semiconductors. Phys Rev B 1970;1:4005–11.
[44] Bouarissa N. Elastic constants and acoustical phonon properties of $GaAsxSb_{1-x}$. Mater Chem Phys 2006;100:41–7.
[45] Baranowski JM. Bond lengths, force constants and local impurity distortions in semiconductors. J Phys C 1984;17:6287.
[46] Bouarissa N, Bachiri R. Elastic constants and related properties of $Al_xGa_{1-x}As_ySb_{1-y}$/InAs. Physica B 2002;322:193–200.
[47] Anderson OL. A simplified method for calculating the Debye temperature from elastic constants. J Phys Chem Solids 1963;24:909–17.
[48] Wortman JJ, Evans RA. Young's modulus, shear modulus, and Poisson's ratio in silicon and germanium. J Appl Phys 1965;36:153–6.
[49] Christmas UME, Faux DA, Cowern NEB. Elastic interaction energy between a silicon interstitial and a carbon substitutional in a silicon crystal. Phys Rev B 2007;76:205205–10.
[50] McSkimin HJ. Measurement of elastic constants at low temperatures by means of ultrasonic waves-data for silicon and germanium single crystals, and for fused silica. J Appl Phys 1953;24:988–97.
[51] Morin FJ, Maita JP. Electrical properties of silicon containing arsenic and boron. Phys Rev 1954;96:28–35.
[52] Montagna M, Dusi R. Raman scattering from small spherical particles. Phys Rev B 1995;52:10080–9.
[53] Moatadid A, Vaissiere JC, Nougier JP. Effect of the degeneracy on the transport of hot holes in silicon. Solid-State Electron 1989;32:1895–9.
[54] Schroeder DV. An introduction to thermal physics. San Francisco: Addison-Wesley; 2000.